Spectral Stability of Deep Two-Dimensional Gravity-Capillary Water Waves

By B. Akers and D. P. Nicholls

In this contribution we study the spectral stability problem for periodic traveling gravity-capillary waves on a two-dimensional fluid of infinite depth. We use a perturbative approach that computes the spectrum of the linearized water wave operator as an analytic function of the wave amplitude/slope. We extend the highly accurate method of Transformed Field Expansions to address surface tension in the presence of both simple and repeated eigenvalues, then numerically simulate the evolution of the spectrum as the wave amplitude is increased. We also calculate explicitly the first nonzero correction to the flat-water spectrum, which we observe to accurately predict the stability (or instability) for all amplitudes within the disk of analyticity of the spectrum. With this observation in mind, the disk of analyticity of the flat state spectrum is numerically estimated as a function of the Bond number and the Bloch parameter, and compared to the value of the wave slope at the first finite amplitude eigenvalue collision.

1. Introduction

Free-surface potential flows arise in a wide array of fluid mechanical problems of engineering interest, for instance, tsunami propagation, the motion of sandbars, and pollutant transport. Due to their ability to propagate energy, momentum, and passive scalars (e.g., pollutants) around the world's oceans, the traveling

Address for correspondence: Benjamin Akers, Air Force Institute of Technology, 2950 Hobson Way, WPAFB, OH 45433; e-mail: benjamin.akers@afit.edu

DOI: 10.1111/j.1467-9590.2012.00574.x

STUDIES IN APPLIED MATHEMATICS 130:81–107

wave solutions are of great interest, and the spectral stability of such solutions under the influence of gravity and capillarity is the topic of this contribution.

This problem has a rich history of both numerical and asymptotic investigation, and the *Annual Review of Fluid Mechanics* is filled with articles summarizing various aspects of the field (see [1] for a particularly relevant and well-written example). The field appears to have begun with Stokes who first expanded periodic traveling water waves as a function of the wave slope in 1845 [2], an approach which has since become commonplace [see, e.g., 3–7].

Regarding dynamic stability of these waveforms, real progress began in the 1960s with the discovery of the Benjamin–Feir instability [8] and, of particular relevance to this study, the amplitude expansions which led to the development of Resonant Interaction Theory (RIT) by Phillips [9] and Benney [10] (for an excellent review of the history of RIT see [11]). In RIT, the dynamics of the solution are predicted, asymptotically in the wave slope, by equations for the amplitudes of a small set of resonantly interacting frequencies, called triad or quartet equations (based on the number of frequencies in the interaction). For traveling water waves, RIT predicts the existence and growth rates of instabilities at frequencies which satisfy such interactions. Numerical studies have computed instabilities in the neighborhood of such resonant interactions, for example, the Class I and Class II instabilities of [12]. Our goal in this paper is to verify numerically that these results are reproducible in the *full* Euler equations of free-surface ideal fluid flow under the influence of gravity and capillarity.

To our knowledge, all stability studies to date concerning traveling wave solutions of the full water wave problem are numerical in nature. Further, almost all of these entail the linearization of the water wave equations about a *fixed* traveling wave solution followed by the numerical approximation of the resulting eigenvalue problem. Please see the classic results of [13, 14] and the more recent computations of [15, 16] for these *spectral* stability analyses.

By contrast to these "Direct Numerical Simulations" (DNS), the authors have embarked on an investigation of spectral stability using a rather different philosophy. In short, it was shown in [17] that the spectrum of the water wave operator linearized about the analytic family of traveling waves [7, 18] is also analytic so that the eigenpair (λ, w) can be expanded in the strongly convergent Taylor series

$$\lambda = \lambda(\varepsilon) = \sum_{n=0}^{\infty} \lambda_n \varepsilon^n, \quad w = w(x;\varepsilon) = \sum_{n=0}^{\infty} w_n(x)\varepsilon^n.$$

These $\{\lambda_n, w_n\}$ have been approximated using the stable and highly (spectrally) accurate [19] method of "Transformed Field Expansions" (TFE), which was used to such great effect by one of the authors with F. Reitich [18, 7] to simulate the underlying traveling waves. We refer the interested reader to

[7] in particular for demonstrations of the capabilities of the TFE approach versus other Boundary Perturbation Methods including its favorable operation counts, lack of substantial numerical ill-conditioning, and applicability to *large* traveling wave profiles via numerical analytic continuation.

To put the present contribution into context we summarize our previous results:

1. In [17] it was demonstrated that the spectrum of the water wave operator linearized about periodic traveling waves is *analytic* as a function of the wave height/slope parameter ε in the absence of resonance (i.e., repeated eigenvalues).
2. In [20] a TFE implementation of the theorem in [17] was used to numerically study the "evolution" of the spectrum for two-dimensional gravity waves. The role of singularities (in the Taylor series) in development of instability from the simple eigenvalue case was investigated.
3. In [21] some conjectures regarding singularities in the spectrum and instability were resolved by comparing with a DNS of the spectrum in the gravity wave case.
4. In [22] the TFE method was extended to the crucially important case of repeated eigenvalues. As we see, RIT correctly tells us that these configurations give rise to the "first" instabilities, those which arise at smallest wave slope.
5. In [19] a rigorous numerical analysis of the TFE recursions was studied in a wide array of contexts, including the spectral stability problem we consider here.

In this study we augment this line of results by:

1. Performing a nontrivial generalization of the TFE approach to spectral stability which accommodates effects of capillarity,
2. Computing *explicitly* the first nonzero correction to the spectrum, λ_1 or λ_2, from an alternate formulation of the potential flow equations. As we will see, this recovers the predictions of RIT and serves as the basis for comparison with TFE simulations,
3. Estimating the disk of analyticity of the spectrum $\{\lambda, w\} = \{\lambda(\varepsilon), w(x;\varepsilon)\}$ from our numerical computations using both (1) the growth rates of the relevant Taylor coefficients and (2) the first uncanceled pole of a Padé approximant,
4. Comparing these results on the disk of analyticity to the first finite amplitude eigenvalue collision using a quadratic approximation to the spectrum (with exactly calculated correction λ_1 or λ_2). Here we observe that the spectrum loses analyticity in the neighborhood of the Wilton ripple at Bond number 0.5, as well in the neighborhood of the Benjamin–Feir and Class I instability curves.

The paper is organized as follows: In Section 2 we discuss a general framework for conducting a spectral stability analysis which not only introduces notation, but also discusses the concept of Bloch periodicity (Section 2.1) and our analyticity results for traveling waves and the spectrum of the corresponding linearized water wave operator (Section 2.2). In Section 3 we present details specific to the water wave problem, with the TFE method discussed in Section 3.1, the DNS in Section 3.2, and the cubic model equation in Section 3.3. It is in this cubic model that the connection between resonances and the structure of the spectrum is presented. We discuss triad resonances in Section 3.4, degenerate quartet resonances in Section 3.5, and nondegenerate quartet resonances in Section 3.6. In Section 4 we present our numerical results including the convergence rate of the method (Section 4.1), the disk of analyticity of the spectrum (Section 4.2), as well as the computed instabilities (Section 4.3). Conclusions and future areas of research are discussed in Section 5.

2. Spectral stability: a general framework

Before discussing the specifics of the water wave problem, we begin with the general framework we employ for our spectral stability study. Consider the generic dynamical system

$$\partial_t v = H(v), \quad v = v(x,t),$$

where H may depend on $x \in \mathbf{R}^d$ and t. Changing to a reference frame traveling uniformly with velocity $c \in \mathbf{R}^d$ we derive the evolution equation

$$\partial_t v + c \cdot \partial_x v = H(v). \tag{1}$$

Suppose that we have *steady* (i.e., traveling wave) solutions to (1), $\{\bar{c}, \bar{v}(x)\}$, which satisfy

$$\bar{c} \cdot \partial_x \bar{v} = H(\bar{v}) \tag{2}$$

and study the evolution of the spectral stability form

$$v(x,t) = \bar{v}(x) + \delta e^{\lambda t} w(x), \quad \delta \ll 1.$$

The parameter λ dictates the linear stability of the traveling wave $\{\bar{c}, \bar{v}\}$ (e.g., if the real part of λ is positive then the wave is linearly unstable) while the function w dictates the spatial dependence of the perturbation. Inserting this form into (1), canceling terms at order zero in δ, equating linear terms, and dropping terms of higher order, we derive the spectral stability problem

$$[H_v(\bar{c}, \bar{v}) - \bar{c} \cdot \partial_x] w = \lambda w,$$

which we abbreviate as

$$\mathcal{A}w = \lambda w, \quad \mathcal{A} = \mathcal{A}(\bar{c}, \bar{v}). \tag{3}$$

2.1. Bloch periodicity

Now, a question of *fundamental* importance arises: Which boundary conditions should w satisfy? If, as we assume here, the traveling wave is periodic then it is natural to assume that w is as well. However, this restrictive (superharmonic) condition will only tell us part of the story [13] and we need a more general class to recover instabilities, e.g., the Benjamin–Feir [8], to waves of *longer* periods [14]. It is standard in these stability studies to consider Bloch (quasi) periodicity [23, 24]: If $\bar{v}$ is periodic with respect to the lattice Γ,

$$\bar{v}(x + \gamma) = \bar{v}(x), \quad \forall \gamma \in \Gamma,$$

then we impose the condition

$$w(x + \gamma) = e^{ip\cdot\gamma} w(x), \quad p \in \mathbf{R}^d, \quad \forall \gamma \in \Gamma.$$

We note that this permits perturbations of quite general periodicities (e.g., if $d = 1$ and waves are 2π-periodic, then $p = 1/2$ permits $w(x)$, which is 4π-periodic) and even those that are *not* periodic. Fortunately, it is well known [23] that, due to periodicity of the spectrum, it suffices to consider a bounded subset of the Bloch (quasi) periods p. For instance, for 2π-periodic functions ($d = 1$) one only need consider the set $\{0 \le p < 1\}$ of Bloch (quasi) periods.

2.2. Analytic dependence of the spectrum

At this point we diverge from other numerical studies of spectral stability for water waves. Given a computed traveling wave solution pair $\{\bar{c}, \bar{v}\}$, these discretize the eigenvalue problem (3) for this particular traveling wave, then compute the spectrum via a standard eigensolver (e.g., the QR algorithm). Not only must this be *recomputed* for each waveform (giving rise to a linear cost in the number of traveling waves simulated), but also any information regarding how the spectrum evolved from the previous state is lost.

By contrast, we use the fact that the traveling waves come in *analytic* families [7, 18]

$$\{\bar{c}, \bar{v}\} = \{\bar{c}, \bar{v}(x)\}(\varepsilon) = \{c_0, 0\} + \sum_{n=1}^{\infty} \{c_n, v_n(x)\}\varepsilon^n,$$

so that the linear operator $\mathcal{A}$ can be expanded

$$\mathcal{A} = \mathcal{A}(\varepsilon) = \sum_{n=0}^{\infty} \mathcal{A}_n \varepsilon^n.$$

We posit that the *spectrum* is also analytic in the *same* parameter (see [17] for a rigorous justification) so that the following are strongly convergent

$$\{\lambda, w\} = \{\lambda, w(x)\}(\varepsilon) = \sum_{n=0}^{\infty} \{\lambda_n, w_n(x)\} \varepsilon^n.$$

Inserting these into (3) and equating at like orders we find

$$(\mathcal{A}_0 - \lambda_0)\, w_n = -(\mathcal{A}_n - \lambda_n)\, w_0 - \sum_{m=1}^{n-1} (\mathcal{A}_{n-m} - \lambda_{n-m})\, w_m.$$

At order $n = 0$ we compute $\{\lambda_0, w_0\}$, which delivers *infinitesimal* spectral stability, while at higher orders we find λ_n such that the right-hand side is in the range of $\mathcal{A}_0 - \lambda_0 I$, and then solve for w_n. In this way we can compute the *entire* spectrum for all values of ε *simultaneously*. This not only saves us from recomputing for every new choice of $\{\bar{c}, \bar{v}\}$ (there is no extra cost associated with simulating additional traveling waves), but it also yields *full* information about the evolution of the spectrum as the wave height/slope is increased.

3. Spectral stability of traveling water waves

We apply our perturbative approach to two, equivalent, formulations of the potential flow Equations (4). The two formulations are representative of two popular methods used to address the difficulty of the unknown domain in this free boundary problem. In the first, a combination of a transparent boundary condition and a domain flattening change of variables is used resulting in the TFE method (Section 3.1). This TFE approach (justified in [17] and, numerically, in [19]) is used to numerically calculate the spectrum, as in [20–22]. In the second formulation (Sections 3.2 & 3.3), the free surface boundary conditions of (4) are expanded about the undisturbed depth, and the problem is then reformulated in terms of surface variables using the Dirichlet–Neumann operator (DNO) as in [25–27]. This latter model is used to calculate *exactly* the leading order correction to the flat state spectrum, λ_1 or λ_2. A brief derivation of both formulations in presented in the following sections.

The widely accepted model for the motion of waves on the surface of a large body of water are the Euler equations of ideal fluid flow [28]

$$\phi_{xx} + \phi_{zz} = 0, \qquad z < \varepsilon\eta, \tag{4a}$$

$$\phi_z \to 0, \quad z \to -\infty, \tag{4b}$$

$$\eta_t + \varepsilon \eta_x \phi_x = \phi_z, \quad z = \varepsilon\eta, \tag{4c}$$

$$\phi_t + \frac{\varepsilon}{2}\left(\phi_x^2 + \phi_z^2\right) + \eta - \sigma \partial_x \left(\frac{\partial_x \eta}{(1 + \varepsilon^2(\partial_x \eta)^2)^{1/2}} \right) = 0, \quad z = \varepsilon\eta, \tag{4d}$$

where η is the free-surface displacement, ϕ is the velocity potential, and $\sigma = \gamma/(gL^2)$ is the Bond number which compares surface tension to gravity forces (γ is the surface tension coefficient, g is the gravitational constant, and L is a typical length scale). These equations describe the motion of an inviscid incompressible fluid on deep water undergoing an irrotational motion. System (4) has been nondimensionalized as in [22, 29] and we assume that the wave slope, $\varepsilon = a/L$ is small (L is chosen in the nondimensionalization so that the waves have spatial period 2π).

The potential flow equations support traveling solutions which depend analytically on ε (see [18] and the references therein), moreover, in the case of simple eigenvalues, the spectral stability problem has eigenvalues and eigenfunctions which also depend analytically on ε [20]. In [22] the authors extended this approach to the case of eigenvalues of higher multiplicity and used this to numerically compute the spectrum of traveling waves as a function of ε. In this work we extend the method to the case of nonzero surface tension.

To describe the TFE approach, we recall the standard (see, e.g., [22]) truncation of the water wave domain to $\{-a < z < \varepsilon\eta\}$, and the *equivalent* formulation of the governing Equations (4):

$$\phi_{xx} + \phi_{zz} = 0, \quad -a < z < \varepsilon\eta, \tag{5a}$$

$$\phi_z - T[\phi] = 0, \quad z = -a, \tag{5b}$$

$$\eta_t + \varepsilon \eta_x \phi_x = \phi_z, \quad z = \varepsilon\eta, \tag{5c}$$

$$\phi_t + \frac{\varepsilon}{2}\left(\phi_x^2 + \phi_z^2\right) + \eta - \sigma \partial_x \left(\frac{\partial_x \eta}{(1 + \varepsilon^2(\partial_x \eta)^2)^{1/2}} \right) = 0, \quad z = \varepsilon\eta, \tag{5d}$$

where the order one Fourier multiplier (a DNO at $y = a$) is given by

$$T[\psi(x)] = T\left[\sum_k \hat{\psi}_k e^{ikx}\right] := \sum_k |k|\, \hat{\psi}_k e^{ikx};$$

here $\hat{\psi}_k$ is the kth Fourier coefficient of $\psi(x)$

$$\psi(x) = \sum_k \hat{\psi}_k e^{ikx}.$$

3.1. Transformed field expansions

To specify the TFE recursions we consider the domain-flattening change of variables

$$x' = x, \quad z' = a\left(\frac{z-\varepsilon\eta}{a+\varepsilon\eta}\right),$$

which are known as σ-coordinates [30] in atmospheric science and the C-method [31] in the electromagnetic theory of gratings. Defining the transformed potential

$$u(x', z') := \phi\left(x', \frac{(a+\varepsilon\eta)z'}{a} + \varepsilon\eta\right),$$

(5) becomes, upon dropping primes,

$$u_{xx} + u_{zz} = F(x, z; u, \varepsilon\eta), \quad -a < z < 0, \tag{6a}$$

$$u_z - T[u] = J(x; u, \varepsilon\eta), \quad z = -a, \tag{6b}$$

$$\eta_t - u_z = Q(x; u, \varepsilon\eta), \quad z = 0, \tag{6c}$$

$$u_t + \eta - \sigma\eta_{xx} = R(x; u, \varepsilon\eta), \quad z = 0, \tag{6d}$$

where the precise forms for F, J, Q, and R are reported in [29]. The important feature of these inhomogeneities is that if $u = \mathcal{O}(\varepsilon)$ (noting that we already have $\varepsilon\eta = \mathcal{O}(\varepsilon)$) then they are $\mathcal{O}(\varepsilon^2)$.

This TFE formulation now fits into the framework of Section 2 with the choice

$$v(x, t) = (\eta(x, t), u(x, 0, t))^T,$$

and H, implicitly defined by (6). The forms required to produce H and H_v have been faithfully recorded in our previous work [17, 20–22] and we direct the motivated reader to the (tedious) details provided therein. However, as we mentioned in the Introduction, in this work we extend this TFE approach to include surface tension effects. In (6) this term appears in R alone as

$$R = R^g + \sigma C(\partial_x\eta) - \sigma\eta_{xx},$$

where R^g refers to the inhomogeneity in the gravity wave problem, and C, is defined by

$$C(\partial_x\eta) := \partial_x\left[\frac{\partial_x\eta}{\sqrt{1+(\partial_x\eta)^2}}\right].$$

Next we define

$$Z(\partial_x \eta) := \frac{1}{\sqrt{1 + (\partial_x \eta)^2}}$$

so that

$$C(\partial_x \eta) = \partial_x \left[(\partial_x \eta)\ Z(\partial_x \eta) \right]. \tag{7}$$

We note the following convenient formula which will be useful later:

$$Z^2 + (\partial_x \eta)^2 Z^2 = 1. \tag{8}$$

For the perturbative TFE method we will need the nth Taylor coefficients of both C and its first variation with respect to η in the ζ direction (the η-component of w) which, from (7), can be expressed as

$$C_\eta(\partial_x \eta)\{\zeta\} = \partial_x \left[(\partial_x \zeta)\ Z(\eta) \right] + \partial_x \left[(\partial_x \eta)\ Z_\eta(\partial_x \eta)\{\zeta\} \right], \tag{9}$$

where, from (8),

$$Z_\eta(\partial_x \eta)\{\zeta\} + (\partial_x \eta)^2 Z_\eta(\partial_x \eta)\{\zeta\} = -Z(\partial_x \eta)(\partial_x \zeta). \tag{10}$$

Based upon the expansions of η and ζ,

$$\varepsilon \eta = \sum_{n=1}^{\infty} \zeta_n(x) \varepsilon^n, \quad \zeta = \sum_{n=0}^{\infty} \zeta_n(x) \varepsilon^n,$$

we seek to find the terms in the Taylor series expansion of C

$$C = C(\eta; \varepsilon) = \sum_{n=1}^{\infty} C_n(x) \varepsilon^n,$$

and C_η

$$C_\eta = C_\eta(\eta; \varepsilon) = \sum_{n=0}^{\infty} C_{\eta,n}(x) \varepsilon^n.$$

To derive the $\{C_n, C_{\eta,n}\}$ we will utilize the expansions of Z

$$Z = Z(\eta; \varepsilon) = \sum_{n=0}^{\infty} Z_n(x) \varepsilon^n,$$

and Z_η

$$Z_\eta = Z_\eta(\eta; \varepsilon) = \sum_{n=0}^{\infty} Z_{\eta,n}(x) \varepsilon^n,$$

and the coefficients $\{Z_n, Z_{\eta,n}\}$.

To begin, we note that from (7)

$$C_n(x) = \sum_{l=1}^{n} \partial_x \left[(\partial_x \eta_l)\ Z_{n-l} \right],$$

while from (9)

$$C_{\eta,n} = \sum_{l=0}^{n} \partial_x \left[(\partial_x \zeta_l)\ Z_{n-l} \right] + \sum_{l=1}^{n} \partial_x [(\partial_x \eta_l) Z_{\eta,n-l}].$$

Thus, we are done if we can identify forms for the Z_n and $Z_{\eta,n}$. For the former we appeal to the formulas from Akers & Nicholls [29], which can be derived from (8), and give $Z_0 = 1$ and (for $n > 0$)

$$\sum_{l=0}^{n} Z_{n-l} Z_l + \sum_{m=0}^{n-2} \sum_{q=0}^{m} \sum_{l=0}^{q} (\partial_x \eta_{n-m-1})(\partial_x \eta_{m+1-q}) Z_{q-l} Z_l = 1.$$

This leads to

$$2 Z_0 Z_n = -\sum_{l=1}^{n-1} Z_{n-l} Z_l - \sum_{m=0}^{n-2} \sum_{q=0}^{m} \sum_{l=0}^{q} (\partial_x \eta_{n-m-1})(\partial_x \eta_{m+1-q}) Z_{q-l} Z_l,$$

and

$$Z_n = -\frac{1}{2} \sum_{l=1}^{n-1} Z_{n-l} Z_l - \frac{1}{2} \sum_{m=0}^{n-2} \sum_{q=0}^{m} \sum_{l=0}^{q} (\partial_x \eta_{n-m-1})(\partial_x \eta_{m+1-q}) Z_{q-l} Z_l.$$

On the other hand, from (10) we have

$$Z_{\eta,n} + \sum_{m=0}^{n-2} \sum_{q=0}^{m} (\partial_x \eta_{n-m-1})(\partial_x \eta_{m+1-q}) Z_{\eta,q} = -\sum_{m=0}^{n-1} \sum_{q=0}^{m} (\partial_x \eta_{n-m})(\partial_x \zeta_{m-q}) Z_q$$

giving

$$Z_{\eta,n} = -\sum_{m=0}^{n-2} \sum_{q=0}^{m} (\partial_x \eta_{n-m-1})(\partial_x \eta_{m+1-q}) Z_{\eta,q} - \sum_{m=0}^{n-1} \sum_{q=0}^{m} (\partial_x \eta_{n-m})(\partial_x \zeta_{m-q}) Z_q.$$

3.2. Direct numerical simulation

In an effort to validate this TFE procedure, in Section 4 we compare TFE simulations to those of a competing method for calculating the spectrum: A DNS method outlined in [21]. This approach, which computes the spectrum for discrete values of the wave height/slope parameter ε, uses Zakharov's surface formulation of the water wave problem [32] in terms of variables $\eta(x, t)$ and

$$\xi(x, t) := \phi(x, \eta(x, t), t),$$

the *surface* velocity potential. This formulation was made more explicit by Craig & Sulem [33], with the introduction of the DNO,

$$G(\eta)\xi := (\partial_z\phi - (\partial_x\eta)\partial_x\phi)_{z=\eta},$$

which maps Dirichlet data, ξ, to Neumann data at the interface η. In terms of this operator the evolution Equations (4) can be *equivalently* stated as

$$\partial_t\eta = G(\eta)\xi, \tag{11a}$$

$$\partial_t\xi = -\eta + \sigma\eta_{xx} - A(\eta)B(\eta,\xi), \tag{11b}$$

where

$$A(\eta) = \frac{1}{2(1+(\partial_x\eta)^2)}, \tag{11c}$$

$$\begin{aligned} B(\eta,\xi) = {} & (\partial_x\xi)^2 - (G(\eta)\xi)^2 - 2(\partial_x\eta)(\partial_x\xi)G(\eta)\xi \\ & + \sigma\partial_x\left(\frac{\partial_x\eta}{(1+\varepsilon^2(\partial_x\eta)^2)^{1/2}} - \partial_x\eta\right). \end{aligned} \tag{11d}$$

This now fits into our general framework of Section 2 with the choice

$$v(x,t) = (\eta(x,t), \xi(x,t))^T,$$

and

$$H(v) = \begin{pmatrix} G(\eta)\xi \\ -\eta + \sigma\eta_{xx} - A(\eta)B(\eta,\xi) \end{pmatrix}$$

We refer the interested reader to [21] for the full details, including the fundamental difficulty of computing the first variation of the DNO (see also [34, 35]).

3.3. A cubic model equation

To further investigate the capabilities of the TFE formulation for simulating the spectrum of the linearized water wave operator, we also compute exactly the first nonzero correction to the flat state spectrum. For this, it is much more convenient to use a cubic approximation to the system (4), see [27]. This approximation (equivalent to the order we require) is based on a Taylor expansion of the free-surface boundary conditions about the undisturbed depth, resulting in two new free surface boundary conditions at $z = 0$:

$$\eta_t - \phi_z + \varepsilon\partial_x\left(\sum_{n=0}^{\infty}\frac{\varepsilon^n}{(n+1)!}\eta^{n+1}\partial_z^n\partial_x\phi\right) = 0, \quad \text{at } z = 0, \tag{12a}$$

$$\phi_t + \eta - \sigma\partial_x\left(\frac{\eta_x}{\left(1+\varepsilon\eta_x^2\right)^{1/2}}\right) + \sum_{n=1}^{\infty}\frac{\varepsilon^n}{n!}\eta^n\partial_z^n\phi_t + \frac{\varepsilon}{2}\left(\sum_{n=0}^{\infty}\frac{\varepsilon^n}{n!}\eta^n\partial_z^n\phi_x^2\right)$$
$$+\frac{\varepsilon}{2}\left(\sum_{n=0}^{\infty}\frac{\varepsilon^n}{n!}\eta^n\partial_z^n\phi_z^2\right) = 0, \quad \text{at } z = 0. \tag{12b}$$

The vertical dependence of the potential can then be solved for as a function of the value of the potential on the free surface, called the surface trace, similar to the procedure for computing the z-derivatives on the artificial boundary of the previous section. Keeping only cubic terms yields

$$\eta_t - \mathcal{L}\Phi + (\eta\Phi_x)_x + \tfrac{1}{2}\left(\eta^2\mathcal{L}\Phi_x\right)_x = 0, \tag{13a}$$

$$\Phi_t + S\eta + \left(\tfrac{1}{2}(\Phi_x)^2 + \tfrac{1}{2}(\mathcal{L}\Phi)^2 + \eta\mathcal{L}\Phi_t\right)$$
$$+\tfrac{1}{2}\left(\sigma(\eta_x)_x^3 + 2\eta(\Phi_x\mathcal{L}\Phi_x - \Phi_{xx}\mathcal{L}\Phi) - \eta^2\Phi_{xxt}\right) = 0. \tag{13b}$$

Where the operators S and $\mathcal{L}$ are defined in terms of their Fourier transform $\hat{S}(k) = 1 + \sigma k^2$ and $\hat{\mathcal{L}}(k) = |k|$, and $\Phi(x,t) \equiv \phi(x,0,t)$ is the trace of the potential at the undisturbed depth. Once again, we appeal to Section 2 with

$$v = (\eta, \Phi)^T$$

and $H = (H^\eta, H^\Phi)$, where

$$H^\eta = \mathcal{L}\Phi - (\eta\Phi_x)_x - \tfrac{1}{2}(\eta^2\mathcal{L}\Phi_x)_x,$$
$$H^\Phi = -S\eta - \left(\tfrac{1}{2}(\Phi_x)^2 + \tfrac{1}{2}(\mathcal{L}\Phi)^2 + \eta\mathcal{L}\Phi_t\right)$$
$$-\tfrac{1}{2}\left(\sigma(\eta_x)_x^3 + 2\eta(\Phi_x\mathcal{L}\Phi_x - \Phi_{xx}\mathcal{L}\Phi) - \eta^2\Phi_{xxt}\right).$$

As we produce rather explicit formulas for the next–order corrections to the terms in the expansion of the spectrum, we write this out (with an abuse of notation by setting the perturbation $w = (\zeta, v)$) in full as

$$\lambda\zeta + c\zeta_x - \mathcal{L}v + Q_1(\eta, \Phi, \zeta, v)_x + \tilde{C}_1(\eta, \Phi, \zeta, v) = 0, \tag{14a}$$

$$\lambda v + cv_x + S\zeta + Q_2(\eta, \Phi, \zeta, v)_x + \tilde{C}_2(\eta, \Phi, \zeta, v) = 0, \tag{14b}$$

where the Q_j are the linearizations of the quadratic terms and the $\tilde{C}_j$ are the linearizations of the cubic terms in (13), whose formulas are given by

$$Q_1 = (\zeta\Phi_x + \eta v_x)_x, \tag{15a}$$

$$\tilde{C}_1 = (\eta\zeta\mathcal{L}\Phi_x)_x + \tfrac{1}{2}\left(\eta^2\mathcal{L}v_x\right)_x, \tag{15b}$$

$$Q_2 = \tfrac{3}{2}\sigma\left(\zeta_x\eta_x^2\right)_x + \zeta(\Phi_x\mathcal{L}\Phi_x - \Phi_{xx}\mathcal{L}\Phi) - c\eta\zeta\Phi_{xxx}, \tag{15c}$$

$$\tilde{C}_2 = \eta(\Phi_x\mathcal{L}v_x - \Phi_{xx}\mathcal{L}v + v_x\mathcal{L}\Phi_x - v_{xx}\mathcal{L}\Phi) - \tfrac{1}{2}\eta^2(\lambda + c\partial_x)v_{xx}. \tag{15d}$$

To begin, a perturbation solution is first computed in Equation (13), via a third-order Stokes expansion as in [22], yielding the traveling Stokes wave

$$\eta = \varepsilon e^{ix} + \varepsilon^2 E_2 e^{2ix} + \ldots *, \tag{16a}$$

$$u = \varepsilon i c_0 e^{ix} + \varepsilon^2 F_2 e^{2ix} + \ldots + *, \tag{16b}$$

$$c = c_0 + \varepsilon c_1 + \varepsilon^2 c_2 + \ldots, \tag{16c}$$

where $*$ refers to the complex conjugate of the preceding terms. The coefficients in (16) are known, see [36, 37], and have been confirmed via rederivation to be

$$\begin{aligned} c_0 &= \sqrt{1+\sigma}, \\ c_1 &= 0, \\ c_2 &= \left(\frac{3\sigma\sqrt{1+\sigma}}{1-2\sigma} + 2\sqrt{1+\sigma} - \frac{3\sigma}{4\sqrt{1+\sigma}} \right), \\ E_2 &= \frac{1+\sigma}{1-2\sigma}, \\ F_2 &= \frac{3i\sigma\sqrt{1+\sigma}}{1-2\sigma}. \end{aligned} \tag{17}$$

Notice that the coefficients c_2, E_2, and F_2 are singular when $\sigma = 0.5$. This value of σ corresponds to a Wilton ripple, in which the leading order wave is in resonance with its first harmonic, and is excluded from this work [38]. Later we will observe the singularity of the coefficients c_2, E_2, and F_2 manifested in a singularity of the spectrum. The spectrum is then determined by substitution of the Stokes wave (16) and the ansatz

$$\zeta = \zeta_0 + \varepsilon\zeta_1 + \varepsilon^2\zeta_2 + \ldots, \tag{18a}$$

$$v = v_0 + \varepsilon v_1 + \varepsilon^2 v_2 + \ldots, \tag{18b}$$

$$\lambda = \lambda_0 + \varepsilon\lambda_1 + \varepsilon^2\lambda_2 + \ldots, \tag{18c}$$

into Equation (14). The corrections λ_1 and λ_2 have been computed when λ_0 has multiplicity one (where ζ_0 is supported at wavenumber k_1) and when λ_0 has multiplicity two (where ζ_0 is supported at wavenumber k_1 and k_2). When the kernel of the linear operator has dimension two, there are three cases, which we categorize by the type of resonance (according to RIT) that occurs between the frequency of the Stokes wave $k_0 = 1$ and the frequencies of the perturbation k_1 and k_2.

The flat state has eigenvalues, $\lambda_0(k) = i\omega[k] - ic_0 k$, where $\omega[k_j]^2 = |k_j|(1+\sigma k_j^2)$. Notice that there are two choices of sign for $\omega[k]$; it need not be positive. A quick calculation reveals that if $\lambda(k_1) = \lambda(k_2)$, then

$$\omega[k_1] - \omega[k_2] = c_0(k_1 - k_2).$$

As frequencies with different Bloch parameter are treated separately, we need only consider collisions between eigenvalues which differ by an integer, and because $k_0 = 1$ and $\omega[k_0] = c_0$, this condition can be written as

$$k_1 - k_2 - nk_0 = 0 \quad \text{and} \quad \omega[k_1] - \omega[k_2] - n\omega[k_0] = 0, \tag{19}$$

thus the existence of a flat state eigenvalue collision implies the existence of a pair of frequencies which are resonant with n instances of the Stokes wave frequency k_0. Because the sign on ω is arbitrary, and ω depends only on the modulus of k and not its sign, it is common to see the equations in (19) with many choices of signs, at the cost of possible redefinitions of the sign of the k_j and $\omega[k_j]$ [39]. In the following sections we observe that the finite amplitude behavior of these collisions depends critically on the value of n. We begin with the case where the wavenumbers of the perturbations differ by one, the triad case.

3.4. Triad resonances

According to RIT, if three wavenumbers satisfy

$$k_1 - k_2 = k_0 \quad \text{and} \quad \omega[k_1] - \omega[k_2] = \omega[k_0],$$

then they are said to take part in a resonant triad [39]. In this case, the leading correction to the flat state spectrum is $\mathcal{O}(\varepsilon)$, and has been computed

$$\lambda_1 = \pm\frac{1}{2}\sqrt{\left(A_2^+ - \frac{\omega[k_1]}{1+\sigma k_1^2}B_2^+\right)\left(A_1^- - \frac{\omega[k_2]}{1+\sigma k_2^2}B_1^-\right)}, \tag{20}$$

where the k_j are labeled so that $k_1 = k_2 + 1$ and the $A_j^{\pm}$ and $B_j^{\pm}$ are the projections of the forcing terms in the equation for ζ_2 and v_2 on the modes $e^{i(k_j \pm 1)x}$:

$$A_1^+ = -i(k_1+1)\left(\frac{k_1\omega[k_1]}{|k_1|} + c_0\right),$$

$$A_1^- = -i(k_1-1)\left(\frac{k_1\omega[k_1])}{|k_1|} + c_0\right),$$

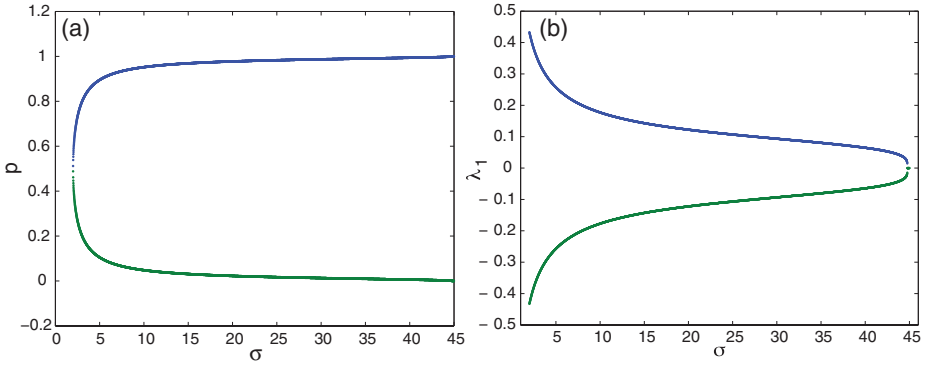

Figure 1. (a) The Bloch parameters, p, for which triad resonances (of the flat state configuration) occur plotted as a function of the Bond number, σ. (b) The first correction λ_1, which is purely real, to the flat state spectrum at the triad-resonant wavenumbers. This figure is colour online.

$$A_2^+ = -i(k_2+1)\left(\frac{k_2\omega[k_2]}{|k_2|}+c_0\right),$$
$$A_2^- = -i(k_2-1)\left(\frac{k_2\omega[k_2]}{|k_2|}+c_0\right),$$
$$B_1^+ = -\left((1+\sigma)(|k_1|-k_1)\frac{\omega[k_1]}{c_0|k_1|}+\omega^2[k_1]+(1+\sigma)\right),$$
$$B_1^- = -\left((1+\sigma)(-|k_1|-k_1)\frac{\omega[k_1]}{c_0|k_1|}+\omega^2[k_1]+(1+\sigma)\right),$$
$$B_2^+ = -\left((1+\sigma)(|k_2|-k_2)\frac{\omega[k_2]}{c_0|k_2|}+\omega^2[k_2]+(1+\sigma)\right),$$
$$B_2^- = -\left((1+\sigma)(-|k_2|-k_2)\frac{\omega[k_2]}{c_0|k_2|}+\omega^2[k_2]+(1+\sigma)\right).$$

For triad resonances, which only occur for σ sufficiently large, the argument of the term under the square root in Equation (20) determines stability. We observe instability for a branch of triads, satisfying Hasselman's criterion [40] whose Bond numbers are in the range $2 < \sigma \lesssim 45$ (see Figure 1). Using the classification scheme of Henderson and Hammack [11], the traveling solutions in this range are considered capillary waves.

3.5. Degenerate quartets

If the waves do not participate in a triad interaction then $\lambda_1 = 0$. In this case, the wavenumbers are part of a quartet and the leading correction to the flat state spectrum is $\mathcal{O}(\varepsilon^2)$. Generally, finding solutions to Equation (19) with the same

Bloch parameter is nontrivial, however one can always find a quartet, by looking at the case when $n = 0$. We refer to this solution as the degenerate quartet,

$$k_0 - k_0 + k_1 - k_1 = 0 \quad \text{with} \quad \omega[k_0] - \omega[k_0] + \omega[k_1] - \omega[k_1] = 0, \tag{21}$$

in which the wave at k_1 interacts with itself. Equation (21) is satisfied trivially at every value of k_1. It is this interaction that determines the leading order correction to λ_0 at every simple eigenvalue, as well as at repeated eigenvalues where the frequencies in the null space have difference larger than twice the Stokes wave frequency; here $k_0 = 1$ thus the latter case refers to waves with $|k_2 - k_1| > 2$. The reason that these two cases have the same asymptotics is that perturbation frequencies which differ by more than twice the Stokes wave frequency do not interact with each other to $\mathcal{O}(\varepsilon^2)$. In carrying out the asymptotics, the leading order eigenfunction, at $\mathcal{O}(1)$, is supported at k_1 and k_2, the next order eigenfunction, at $\mathcal{O}(\varepsilon)$, gains support at $k_1 \pm 1$ and $k_2 \pm 1$, etc. At $\mathcal{O}(\varepsilon^n)$ then, the frequencies of the perturbation can only interact if their difference is less than n. As a result to $\mathcal{O}(\varepsilon^2)$, eigenvalues of multiplicity two whose frequencies differ by more than two behave as two decoupled simple eigenvalues.

For these degenerate quartets, as well as for simple eigenvalues, the leading order correction to the flat state spectrum is

$$\lambda_2 = \frac{i\omega[k_1]}{2\left(1+\sigma k_1^2\right)} T_1 - \frac{1}{2} t_1, \tag{22}$$

where t_1 is the coefficient of the harmonic e^{ik_1x} in the ζ_3 equation and T_1 is the coefficient of e^{ik_1x} in the v_3 equation, whose formulas are

$$\begin{aligned}
t_1 &= ik_1\left(c_2 + i(k_1+1)\Gamma_1 + i(k_1-1)\Gamma_2 - \gamma_1 c_0 - \gamma_2 c_0 - 2c_0 - k_1\omega[k_1]\right), \\
T_1 &= \Bigg(-\frac{c_2 k_1 \omega[k_1]}{|k_1|} - i(k_1+1)c_0\Gamma_1 - i|k_1+1|c_0\Gamma_1 + |k_1+1|(\lambda_0 + ic_0 \\
&\quad \times (k_1+1))\Gamma_1 - \gamma_1(1+\sigma) - i(k_1-1)c_0\Gamma_2 + i|k_1-1|c_0\Gamma_2 \\
&\quad + |k_1-1|(\lambda_0 + ic_0(k_1-1))\Gamma_2 - \gamma_2(1+\sigma) - 3\sigma k_1^2 \\
&\quad + 2(1+\sigma) + 2k_1\omega[k_1]c_0 + 2\frac{k_1 c_0 \omega[k_1]}{|k_1|} - \frac{k_1^2\omega[k_1]^2}{|k_1|}\Bigg).
\end{aligned}$$

The coefficients γ_j and Γ_j are the coefficients of $e^{i(k_1\pm 1)x}$ in the solution ζ_2 and v_2, respectively, with formulas

$$\begin{aligned}
\begin{pmatrix}\gamma_1 \\ \Gamma_1\end{pmatrix} &= \frac{1}{(\omega[k_1]+\omega[1])^2 - \omega^2[k_1+1])} \\
&\quad \times \begin{pmatrix} i(\omega[k_1]+\omega[k_0])A_1^+ + |k_1+1|B_1^+ \\ i(\omega[k_1]+\omega[k_0])B_1^+ - (1+\sigma(k_1+1)^2)A_1^+ \end{pmatrix},
\end{aligned}$$

$$\begin{pmatrix}\gamma_2\\ \Gamma_2\end{pmatrix} = \frac{1}{(\omega[k_1]+\omega[1])^2-\omega^2[k_1-1])} \times \begin{pmatrix} i(\omega[k_1]-\omega[k_0])A_1^- + |k_1-1|B_1^- \\ i(\omega[k_1]-\omega[k_0])B_1^- - (1+\sigma(k_1-1)^2)A_1^-\end{pmatrix}.$$

A brief inspection reveals that λ_2 in Equation (22) is pure imaginary, thus neither simple eigenvalues nor repeated eigenvalues whose frequencies differ by more than two lead to instability to this order. The Class II instabilities of MacKay and Saffman [12] fall into this latter category, and thus do not occur, at least to $\mathcal{O}(\varepsilon^2)$, for two-dimensional deep-water gravity-capillary waves. This result fits with the observation that for gravity waves the Class II instability is fundamentally three dimensional [41]. It is worth noting however that although in this case λ_2 is pure imaginary for all values of p and σ, the disk of analyticity of the spectrum is vanishingly small in the neighborhood of $\sigma = 0$.

3.6. Quartet resonances

Quartets which may lead to instability, to $\mathcal{O}(\varepsilon^2)$, occur at repeated eigenvalues where the frequencies differ by exactly twice the Stokes wave frequency, $2k_0$,

$$k_1 - k_2 = 2k_0 \quad \text{with} \quad \omega[k_1]+\omega[k_2] = 2\omega[k_0].$$

For these quartets, the correction to the flat state eigenvalue is determined from the root of a quadratic,

$$\lambda_2 = \tfrac{1}{2}(P_{2,2}+P_{1,1}) \pm \tfrac{1}{2}\sqrt{(P_{2,2}-P_{1,1})^2+4P_{1,2}P_{2,1}}, \tag{23}$$

where the $P_{j,j}$ are defined as

$$\begin{aligned} P_{1,1} &= \frac{i\omega[k_1]}{2\left(1+\sigma k_1^2\right)}T_1 - \frac{1}{2}t_1,\\ P_{1,2} &= \frac{i\omega[k_1]}{2\left(1+\sigma k_1^2\right)}T_4 - \frac{1}{2}t_4,\\ P_{2,1} &= \frac{i\omega[k_2]}{2\left(1+\sigma k_2^2\right)}T_5 - \frac{1}{2}t_5,\\ P_{2,2} &= \frac{i\omega[k_2]}{2\left(1+\sigma k_2^2\right)}T_2 - \frac{1}{2}t_2. \end{aligned}$$

The $P_{j,j}$ are computed by enforcing solvability of the equations for ζ_3 and v_3, i.e., that the forcing terms in the equations for v_3 and ζ_3 are orthogonal the null space of the linear operator. It is simple to see that these $P_{j,j}$ are pure imaginary, and thus stability is determined, to $\mathcal{O}(\varepsilon^2)$, by the discriminant in Equation (23). The t_4, t_5 are the coefficients of the harmonics $e^{i(k_2+2)x}$ and $e^{i(k_1-2)}$ in the equation for ζ_3, while T_4 and T_5 are the corresponding coefficients of these same harmonics in the equation for v_3. These coefficients

have been computed to be

$$t_4 = i(k_2+2)\left(i(k_2+1)\Gamma_3 - \gamma_3 c_0 + 2iF_2 - E_2\frac{k_2\omega[k_2]}{|k_2|} - c_0 - \frac{1}{2}\omega[k_2]k_2\right),$$

$$t_5 = i(k_1-2)\left(i(k_1-1)\Gamma_2 - \gamma_2 c_0 - 2i\bar{F}_2 - \bar{E}_2\frac{k_1\omega[k_1]}{|k_1|} - c_0 - \frac{1}{2}\omega[k_1]k_1\right),$$

$$\begin{aligned} T_4 = {} & (-i(k_2+1)\Gamma_3 c_0 + i|k_2+1|\Gamma_3 c_0 + |k_2+1|(\lambda_0 + ic_0(k_2+1))\Gamma_3 \\ & - (1+\sigma)\gamma_3 - \frac{2k_2F_2(i\omega[k_2])}{|k_2|} + 2i\omega[k_2]F_2 - E_2\omega[k_2]^2 + 4ic_0F_2 \\ & + \frac{3}{2}\sigma k_2(k_2+2) - (1+\sigma)k_2\omega[k_2]c_0 - \omega[k_2]c_0 + \frac{k_2c_0\omega[k_2]}{|k_2|} \\ & - \frac{k_2^2\omega[k_2]c_0}{|k_2|} - \frac{k_2^2\omega[k_2]^2}{2|k_2|}\Bigg), \end{aligned}$$

$$\begin{aligned} T_5 = {} & (-i(k_1-1)c_0\Gamma_2 - i|k_1-1|c_0\Gamma_2 + |k_1-1|(\lambda_0 + ic_0(k_1-1))\Gamma_2 \\ & - (1+\sigma)\gamma_2 + \frac{2ik_1\bar{F}_2\omega[k_1]}{|k_1|} + 2i\bar{F}_2\omega[k_1] - \bar{E}_2\omega[k_1]^2 - 4ic_0\bar{F}_2 \\ & + \frac{3}{2}\sigma k_1(k_1-2) - (1+\sigma)k_1\omega[k_1]c_0 + \omega[k_1]c_0 + \frac{k_1c_0\omega[k_1]}{|k_1|} \\ & + \frac{k_1^2c_0\omega[k_1]}{|k_1|} - \frac{k_1^2\omega[k_1]^2}{2|k_1|}\Bigg). \end{aligned}$$

The coefficients γ_j and Γ_j are the coefficients of $e^{i(k_2\pm1)x}$ in the solution ζ_2 and v_2, respectively, with formulas

$$\begin{aligned} \begin{pmatrix}\gamma_3\\ \Gamma_3\end{pmatrix} = {} & \frac{1}{(\omega[k_2]+\omega[k_0])^2 - \omega^2[k_2+1]} \\ & \times \begin{pmatrix} i(\omega[k_2]+\omega[k_0])A_2^+ + |k_2+1|B_2^+ \\ i(\omega[k_2]+\omega[k_0])B_2^+ - (1+\sigma(k_2+1)^2)A_2^+ \end{pmatrix}, \\ \begin{pmatrix}\gamma_4\\ \Gamma_4\end{pmatrix} = {} & \frac{1}{(\omega[k_2]-\omega[k_0])^2 - \omega^2[k_2-1]} \\ & \times \begin{pmatrix} i(\omega[k_2]-\omega[k_0])A_2^- + |k_2-1|B_2^- \\ i(\omega[k_2]-\omega[k_0])B_2^- - (1+\sigma(k_2-1)^2)A_2^- \end{pmatrix}. \end{aligned}$$

Excepting that here the formulas are more complicated, these corrections are determined by the same procedure as that in [22], in which the calculation of λ_2 without surface tension appears.

In the TFE method of Section 3.1, the solvability conditions to find the first nonzero λ_n are the same as in the above exact calculation. The solvability conditions for all later orders values of λ_n are linear, and the equations can

be solved to arbitrary order thus, formally, a solution exists. In the next section we present the numerical results of this method, including the radius of convergence of the series expansion of the eigenvalues.

4. Numerical results

In this section we summarize the results of numerical simulations based on three approaches to the spectral stability problem for gravity-capillary water waves:

1. A numerical method based on the TFE formulation of the potential flow equations is used to compute the corrections to the spectrum to arbitrary perturbation order N (Section 3.1);
2. A DNS based upon Zakharov and Craig & Sulem's formulation of the water wave problem (Section 3.2);
3. A computation of the first nonzero correction to the spectrum, directly from the cubic truncation (13) (Section 3.3).

In regards to the first approach, and as we mentioned earlier, we have extended the numerical method developed in [7, 22, 29] to include both surface tension and generic eigenvalues collisions (where the eigenvalues have multiplicity two in the flat state configuration). Furthermore, the domain of applicability of the method is examined by approximating the disk of analyticity of the spectrum. Within this the convergence rate of the numerical method is validated at resonant spectral values. The spectrum itself is examined, with particular focus on the role of resonances in determining spectral stability.

4.1. A brief convergence study

Before embarking upon this study we investigate the consistency of our numerical TFE approach with respect to the DNS algorithm we have devised. In Figure 2 we present both the growth rates of the corrections λ_n at a triad resonant eigenvalue (where λ_0 has multiplicity two and the functions in the null space have frequencies which differ by one), and the error of the TFE method for fixed ε ($\varepsilon = 0.05$). The error is measured by comparing the partial sum of the eigenvalue corrections to the calculations of the nonperturbative DNS calculation,

$$\left| \sum_{m=0}^{n} \lambda_m \varepsilon^m - \lambda_{\mathrm{DNS}} \right|.$$

As is typical inside the disk of analyticity, the convergence is exponential and only a small number of terms are required to achieve machine precision (e.g., in this figure it is sufficient to choose $N \approx 10$).

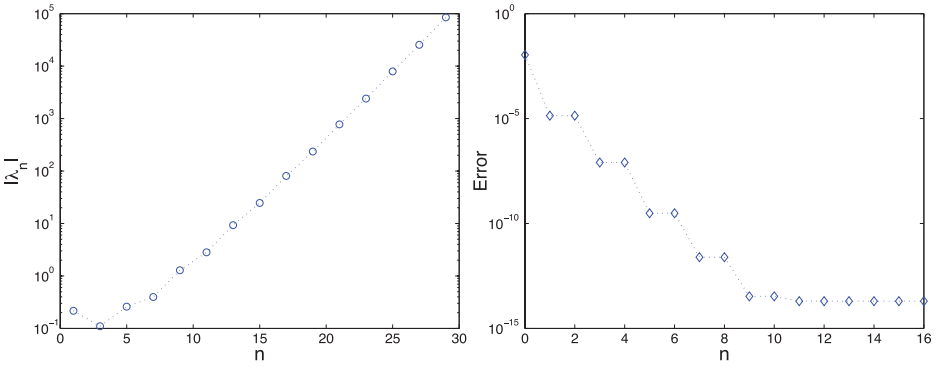

Figure 2. Left-hand side: The size of the corrections λ_n are plotted as a function of the perturbation order n for an eigenvalue which is of multiplicity two for the flat state configuration, $(\sigma, p) = (2, 0.5)$. Right-hand side: The difference between the TFE calculation and the DNS calculation of the spectrum plotted as a function of perturbation order for $\varepsilon = 0.05$. This figure is colour online.

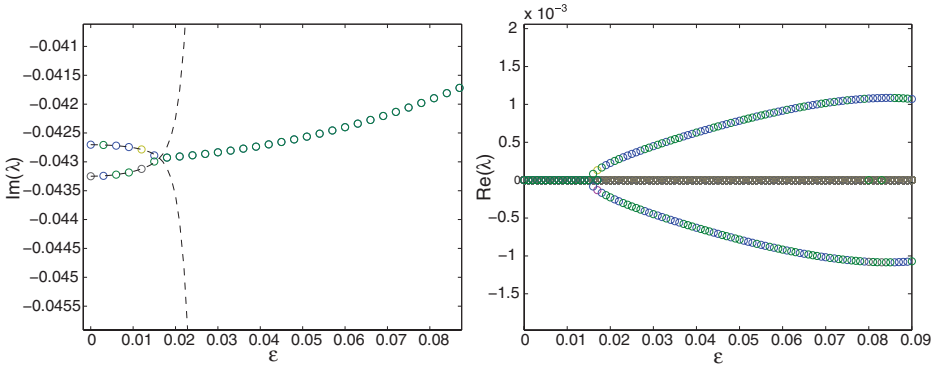

Figure 3. Left-hand side: Two simple pure imaginary eigenvalues collide at finite wave slope $\varepsilon \approx 0.016$. This spectrum is calculated at Bond number $\sigma = 0.12$ and Bloch parameter $p \approx 0.1035$, where the flat state has a quartet resonant eigenvalue $\lambda_0 \approx -0.431i$. The circles are DNS approximations and the dotted lines are results of a TFE simulation. Right-hand side: Real eigenvalues bifurcate from zero at $\varepsilon \approx 0.016$, the result of the collision the eigenvalues in the left panel. Although the TFE method can predict such eigenvalue collisions, it cannot compute "beyond" them as there is a loss of analyticity in ε. This figure is colour online.

4.2. Domain of applicability of the method

In addition to considering the convergence at fixed ε, it is interesting to consider the performance of this method as a function of ε with fixed perturbation order N. In Figure 3, we observe the fit of this method to simple eigenvalues at nonzero Bond number, $\sigma = 0.12$. Notice that the TFE calculation does an excellent job of approximating the spectrum all the way to eigenvalue collision. The configuration of Figure 3, $\sigma = 0.12$ and $p \approx 0.1035$, is a resonant one,

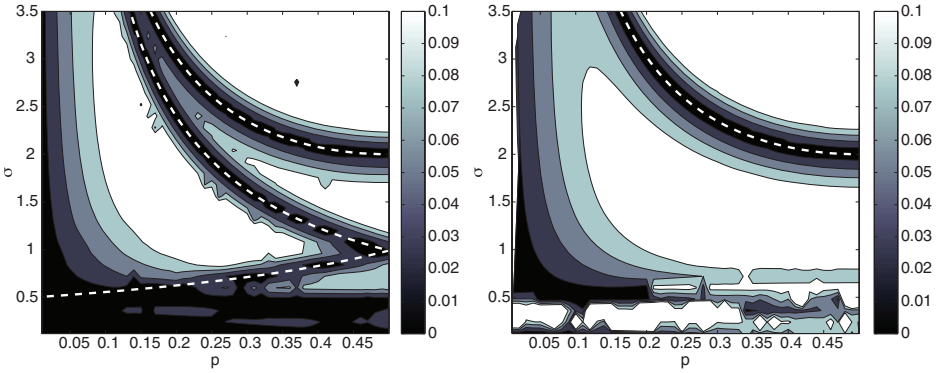

Figure 4. The disk of analyticity of the spectrum is numerically estimated as a function of the Bond number σ and the Bloch parameter p. On the left, the growth rate of the Taylor coefficients is used to estimate the disk of analyticity. On the right, the first noncanceled pole of the Padé expansion is used as an estimate of the disk of analyticity. Triad resonances are marked with dashed white curves, and each of these corresponds to an instability (in the neighborhood of which the disk of analyticity vanishes). The additional triad resonance curves in the left plot do not lead to instability; these triad resonances occur at a collision of eigenvalues of the same Krein signature. The disk of analyticity of the spectrum also vanishes at $\sigma = 0.178$ (the minimum of the group velocity) and $\sigma = 0.5$ (Wilton's Ripple) and near $p = 0$ outside of $0.178 < \sigma < 0.5$ due to the Benjamin–Feir instability. For $\sigma < 0.5$ the dependence on p is also complicated by the accumulation of nonisolated resonances and the higher order Wilton ripples at $\sigma = 1/n$. This figure is colour online.

in that there is an eigenvalue collision at $\varepsilon = 0$, $\lambda_0 \approx 0.431i$. However, this collision is *not* responsible for the loss of analyticity of the spectrum.

For $\sigma < 0.5$, resonances accumulate in the p–σ plane, and both resonances and *near*-resonances are common. The configuration $(p, \sigma) \approx (0.12, 0.1035)$ has a near resonant pair of eigenvalues with $\lambda_0 \approx 0.0425i$ and $\lambda_0 \approx 0.0435i$, which lead to a finite amplitude collision and the loss of analyticity of the spectrum. The remainder of the spectrum remains analytic for much larger ε. In this work we consider the disk of analyticity of the *entire* spectrum, and in later presentations of such we present only the smallest ε for which *any* eigenvalue loses analyticity. Thus the TFE method can, in fact, compute much of the spectrum to *larger* values of ε than this smallest value (reported in Figure 4).

4.3. Disk of analyticity

A novel feature of the TFE method, relative to traditional computations of the spectrum, is the ability to study the disk of analyticity of the spectrum (see Figure 4). To generate Figure 4, the Bloch parameter and Bond number were discretized using uniform spacings $\Delta p = 0.01$ and $\Delta\sigma = 0.12$. For every value of p and σ sampled to create the plot, all of the eigenvalues in the flat

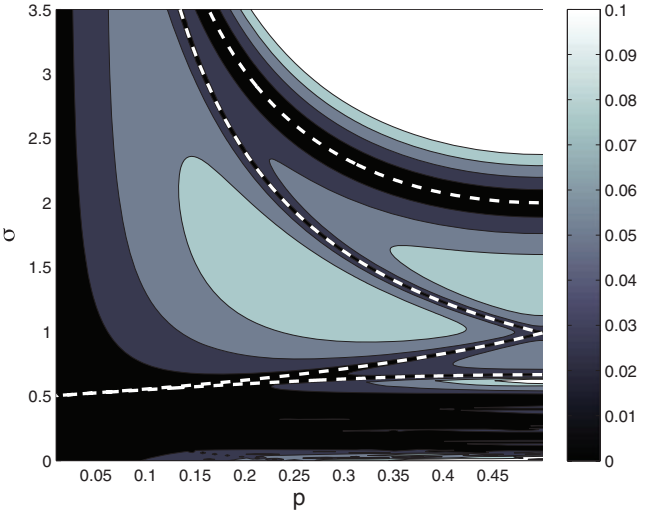

Figure 5. The smallest value of ε for which there is a collision of eigenvalues is calculated using the quadratic approximation $\lambda \approx \lambda_0 + \varepsilon^2\lambda_2$ about simple eigenvalues in the p–σ plane. This approximation predicts collisions of eigenvalues near resonance curves. Four isolated resonances are marked with white dotted lines. The lowermost dashed white curve is an opposite Krein signature quintet resonance. The uppermost dashed curve is an opposite Krein signature triad resonance. The middle two dashed curves are triad resonances of eigenvalues with the same Krein signature. Small amplitude eigenvalue collisions are also predicted for $\sigma < 0.5$, where the resonances accumulate, and near $p = 0$, the Benjamin–Feir instability. This figure is colour online.

state spectrum are simple. In fact, repeated eigenvalues happen on a set of measure zero. The disk of analyticity was then estimated in two ways: First, by estimating the growth rate of the Taylor series coefficients λ_n, and second, by the first noncanceled pole of the diagonal Padé approximant. (Both estimates were made using $N = 24$ terms.)

4.4. Results on stability

It is well known that small ε instabilities occur near resonant configurations (see [1]). Moreover, instabilities arise from resonant configurations only with opposite Krein signature [12]. This necessary condition is known to be insufficient for general collisions [20, 22], but is both necessary and sufficient for triads [40].

In Figure 5 four resonant curves are marked with dashed lines. These curves are, from top to bottom, three resonant triads and a resonant quintet. The uppermost curve is a resonant triad of opposite Krein signature, which results in instability, often referred to as a Class I instability [12]. The leading order growth rate of this instability, λ_1, is plotted in Figure 1. This instability is also evident in the uppermost dark band in both panels of Figure 4. The

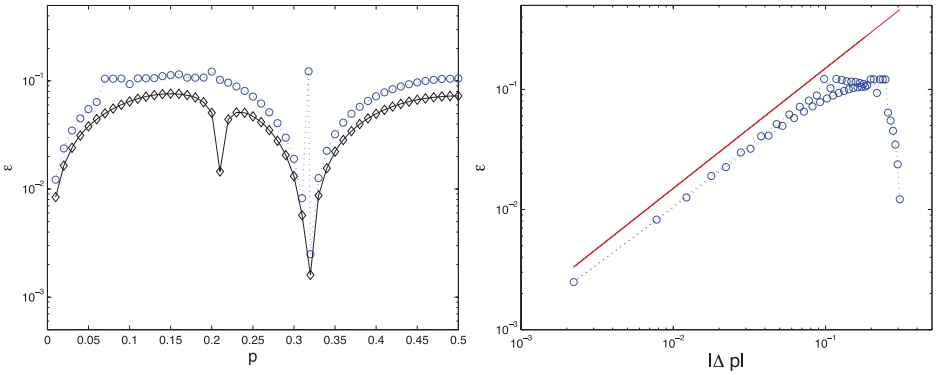

Figure 6. Left-hand side: The disk of analyticity of the spectrum is numerically estimated versus the Bloch parameter p, at fixed $\sigma = 2.28$ (circles) and by the smallest collision of opposite Krein signature eigenvalues using the second-order approximation (diamonds). A triad resonance occurs at $p \approx 0.318$. The numerical estimate of the disk of analyticity uses the first noncanceled pole of the diagonal Padé approximant, as in Figure 4. Notice that the disk of analyticity for fixed p shrinks to zero as p approaches the resonant value, however, at the resonant value of p the spectrum is analytic to much larger radius. Right-hand side: A log–log plot shows that the disk of analyticity near a triad vanishes linearly with distance to the triad Bloch parameter, $|\Delta p| = |p - p^*|$. The radius of convergence is marked with circles as in the left panel. A line of slope one, corresponding to a linear relationship between ε and $|\Delta p|$, is marked by the solid line. As in the left panel, $\sigma = 2.28$ and the triad occurs at the critical $p^* \approx 0.318$. This figure is colour online.

lowermost dashed curve in Figure 5 is quintet resonance of opposite Krein signature, which does not lead to instability, a Class II resonance. Comparing Figures 5 and 4, we also observe that the radius of convergence of the Taylor series shrinks at the three triad resonances (the uppermost of opposite Krein signature, the lower two of the same Krein signature) but does not vanish near the opposite Krein signature quintet resonance of Figure 5. On the other hand, the Padé approximation (presented in the right panel of Figure 4) predicts that the solution does *not* lose analyticity near these lower three resonance curves, only near the uppermost which is an opposite Krein signature triad resonance.

In the immediate neighborhood of the opposite Krein signature resonant triad, the spectrum loses analyticity at small amplitude, where the radius of analyticity scales linearly with distance to the resonant configuration. This loss of analyticity is due to the collision of the two near-resonant, but simple, eigenvalues. In Figure 6 the disk of analyticity is estimated as a function of p at $\sigma = 2.28$ by the first noncanceled pole of the numerically computed series to $N = 30$ orders. Figure 6 is essentially a cross-section of Figure 4, in which we have included the resonant configuration at $p \approx 0.318$. Notice that the disk of analyticity vanishes as p approaches this configuration (linearly in Δp). In this figure, the numerically computed disk of analyticity of the spectrum is

compared to a prediction of the first finite amplitude collision based on the $\mathcal{O}(\varepsilon^2)$ approximation of the spectrum (see Section 3.3 for the derivation of the λ_2) with good agreement.

The ε at which the collision occurs appears to scale linearly in p. This suggests that it may be possible to expand p as a function of ε about the resonant configurations. Such an expansion would allow the current method to compute more instabilities, including the neighborhood of the triad resonance in Figure 4 as well as the Benjamin–Feir instability. Neither of the aforementioned instabilities are analytic in ε for fixed p, and with p fixed both are finite amplitude instabilities. A near-resonant Stokes' expansion, essentially expanding in p, has been successfully applied to compute near-resonant traveling waves to the KdV equation [42]; a similar expansion in the TFE method is an area which is being actively pursued.

4.5. Nonisolated resonances

The structure of the set of resonances of spectrum of traveling waves in the potential flow Equations (4) is quite rich. In addition to the isolated resonances mentioned in the previous paragraphs, the equation supports nonisolated resonances, at which λ_0 has kernel of dimension higher than two. Nonisolated resonances (e.g., where a wavenumber is part of both a triad *and* a quartet), create the "rough" regions in Figure 4. We note that these nonisolated resonances accumulate in the region $\sigma \approx 0$ [43]. It is not clear that an amplitude expansion is the right approach to compute the spectrum in a region where the resonant sets are intertwined in such a complicated manner (as they are in $0 < \sigma \leq 0.5$).

Apart from the triad resonance, the spectrum loses analyticity near the two sets: The Wilton ripple resonance at $\sigma = 0.5$, and the Benjamin–Feir instability at $p = 0$ (outside the interval $\sigma = [0.178, 0.5]$). Both of these regions require nontrivial extension of the current algorithm which currently finds the spectrum of Stokes waves perturbed about eigenvalues of multiplicity one or two.

Wilton's ripple is a traveling wave which bifurcates from a flat state configuration which has a two-dimensional null space [38]. The extension of [29] to compute Wilton ripples and resonant short crested waves with amplitude expansions is currently being pursued. The TFE algorithms of [7, 29] do not currently compute such waves. The Benjamin–Feir instability bifurcates from a collision of flat state eigenvalues of algebraic multiplicity four, also not currently supported by the algorithm [29]. Extending the algorithm to higher dimensional null spaces is not sufficient to compute this instability, however, as for fixed p the instability is either not present ($p = 0$) or not analytic in ε (for p small). For fixed p, the Benjamin–Feir instability can be thought of as being the result of a collision of near-resonant eigenvalues, or "sidebands." The extension of the method to near-resonant eigenvalues is a planned direction of future research as is the finite depth problem.

5. Conclusion

A perturbative numerical method was presented for computing simple and resonant spectra for deep-water gravity-capillary waves, extending previous work on simple and resonant gravity wave spectra. This method assumes analyticity of the spectrum for fixed Bloch parameter p and can be used to numerically approximate the disk of analyticity of the relevant Taylor series. Using a different approach, the leading order asymptotics of the spectrum are also directly calculated and compared with this stable perturbative approach. A branch of unstable triads is observed to be analytically connected to the flat state spectrum, in the neighborhood of which the spectrum is *not* analytic. The analyticity of the spectrum is also studied at other resonant configurations (of Bloch parameter p and Bond number σ). A modulational extension of this method, which expands the Bloch parameter in ε, should allow for the computation of instabilities which are not analytically connected to the flat state at fixed p (e.g., the Benjamin–Feir instability). This extension to near resonances as well as the finite depth problem, are avenues of ongoing research.

References

1. F. Dias and C. Kharif, Nonlinear gravity and gravity-capillary waves, *Ann. Rev. Fluid Mech.* 31:301–346 (1999).
2. A. Craik, George Gabriel Stokes on water wave theory, *Ann. Rev. Fluid Mech.* 37: 23–42 (2005).
3. W. Harrison, The influence of viscosity and capillarity on waves of finite amplitude, *Proc. Lond. Math. Soc.* 7: 107–121 (1909).
4. R. J. C. Kamesvara, On ripples of finite amplitude, *Proc. Indian Ass. Cultiv. Sci.* 6: 175–193 (1920).
5. L. McGoldrick, An experiment on second-order capillary gravity resonant wave interactions, *J. Fluid Mech.* 40: 251–271 (1970).
6. J. Reeder and M. Shinbrot, Three dimensional, nonlinear wave interaction in water of constant depth, *Non. Anal.* 5: 303–323 (1981).
7. D. Nicholls and F. Reitich, Stable, high-order computation of traveling water waves in three dimensions, *Eur. J. Mech. B/Fluids* 25: 406–424 (2006).
8. T. B. Benjamin and J. Feir, The disintegration of wave trains on deep water, *J. Fluid Mech.* 27: 417–430 (1967).
9. O. Phillips, On the dynamics of unsteady gravity waves of finite amplitude. Part 1. The elementary interactions, *J. Fluid Mech.* 9: 193–217 (1960).
10. D. Benney, Non-linear gravity wave interactions, *J. Fluid Mech.* 14: 577–584 (1962).
11. J. L. Hammack and D. M. Henderson, Resonant interactions among surface water waves, *Ann. Rev. Fluid Mech.* 25: 55–97 (1993).
12. R. S. MacKay and P. Saffman, Stability of water waves, *Proc. R. Soc. Lond. A* 406: 115–125 (1986).
13. M. S. Longuet-Higgins, The instabilities of gravity waves of finite amplitude in deep water. I. Superharmonics, *Proc. R. Soc. London Ser. A* 360: 471–488 (1978).

14. M. S. Longuet-Higgins, The instabilities of gravity waves of finite amplitude in deep water. II. Subharmonics, *Proc. R. Soc. London Ser. A* 360: 489–505 (1978).
15. M. Francius and C. Kharif, Three-dimensional instabilities of periodic gravity waves in shallow water, *J. Fluid Mech.* 561: 417–437 (2006).
16. B. Deconinck and K. Oliveras, The instability of periodic surface gravity waves, *J. Fluid Mech.* 675: 141–167 (2011).
17. D. P. Nicholls, Spectral stability of traveling water waves: Analytic dependence of the spectrum, *J. Nonlin. Sci.* 17: 369–397 (2007).
18. D. P. Nicholls and F. Reitich, On analyticity of traveling water waves, *Proc. R. Soc. Lond., A* 461: 1283–1309 (2005).
19. D. P. Nicholls and J. Shen, A rigorous numerical analysis of the transformed field expansion method, *SIAM J. Numer. Anal.* 47: 2708–2734 (2009).
20. D. Nicholls, Spectral data for traveling water waves: Singularities and stability, *J. Fluid Mech.* 624: 339–360 (2009).
21. D. P. Nicholls, Spectral stability of traveling water waves: Eigenvalue collision, singularities, and direct numerical simulation, *Physica D*, 240: 376–381 (2011).
22. B. Akers and D. P. Nicholls, Spectral stability of deep two-dimensional gravity water waves: Repeated eigenvalues, *SIAM J. Appl. Math.* 72: 689–711 (2012).
23. A. Mielke, Instability and stability of rolls in the Swift-Hohenberg equation, *Comm. Math. Phys.* 189: 829–853 (1997).
24. B. Deconinck and J. N. Kutz, Computing spectra of linear operators using the Floquet-Fourier-Hill method, *J. Comput. Phys.* 219: 296–321 (2006).
25. B. Akers and P. Milewski, Model equations for gravity-capillary waves in deep water, *Stud. Appl. Math.* 121: 49–69 (2008).
26. B. Akers and P. Milewski, Dynamics of three dimensional gravity-capillary solitary waves in deep water, *SIAM J. Appl. Math.* 70: 2390–2408 (2010).
27. B. Akers, The generation of capillary-gravity solitary waves by a surface pressure forcing, *Math. Comp. Sim.* 82: 958–967 (2012).
28. H. Lamb, *Hydrodynamics*, Cambridge University Press, New York, 1879.
29. B. Akers and D. P. Nicholls, Traveling waves with gravity and surface tension, *SIAM J. Appl. Math.* 70: 2373–2389 (2010).
30. N. A. Phillips, A coordinate system having some special advantages for numerical forecasting, *J. Atmos. Sci.* 14: 184–185 (1957).
31. J. Chandezon, D. Maystre, and G. Raoult, A new theoretical method for diffraction gratings and its numerical application, *J. Opt.* 11: 235–241 (1980).
32. V. Zakharov, Stability of periodic waves of finite amplitude on the surface of a deep fluid, *J. Appl. Mech. Tech. Phys.* 9: 190–194 (1968).
33. W. Craig and C. Sulem, Numerical simulation of gravity waves, *J. Comput. Phys.* 108: 73–83 (1993).
34. C. Fazioli and D. P. Nicholls, Parametric analyticity of functional variations of Dirichlet–Neumann operators, *Diff. Integ. Eqns.* 21: 541–574 (2008).
35. C. Fazioli and D. P. Nicholls, Stable computation of variations of Dirichlet–Neumann operators, *J. Comput. Phys.* 229: 906–920 (2010).
36. G. Whitham, *Linear and Nonlinear Waves*, Wiley, New York, 1974.
37. W. Pierson and P. Fife, Some nonlinear properties of long-crested periodic waves with lengths near 2.44 centimeters, *J. Geophys. Res.* 66: 163–179 (1961).
38. J. Wilton, On ripples, *Phil. Mag.* 29: 688–700 (1915).
39. A. D. Craik, *Wave Interactions and Fluid Flows*, Cambridge University Press, New York, 1985.

40. K. Hasselmann, A criterion for nonlinear wave stability, *J. Fluid Mech.* 30: 737–739 (1967).
41. J. McLean, Y. Ma, D. Martin, P. Saffman, and H. Yuen, Three-dimensional instability of finite-amplitude water waves, *Phys. Rev. Lett.* 46: 817–820 (1981).
42. S. E. Haupt and J. P. Boyd, Modeling nonlinear resonance: A modification of the Stokes perturbation expansion, *Wave Motion* 10: 83–98 (1988).
43. W. Craig and D. P. Nicholls, Traveling two and three dimensional capillary gravity water waves, *SIAM J. Math. Anal.* 32: 323–359 (2000).

Air Force Institute of Technology
University of Illinois

(Recevied May 3, 2012)